THE ASTROPHYSICAL JOURNAL, 405:538–553, 1993 March 10

SPECTRAL EVOLUTION OF STELLAR POPULATIONS USING ISOCHRONE SYNTHESIS

GUSTAVO BRUZUAL A.
Centro de Investigaciones de Astronomía, AP 264, 5101-A Mérida, Venezuela
AND
STÉPHANE CHARLOT[1]
Space Telescope Science Institute, 3700 San Martin Drive, Baltimore, MD 21218
Received 1991 September 25; accepted 1992 September 17

ABSTRACT

We combine the photometric model of isochrone synthesis recently published by Charlot & Bruzual with an updated library of stellar spectra to predict the spectral evolution of stellar populations with solar metallicity. The library of spectra assembled here supersedes other existing libraries (Bruzual; Guiderdoni & Rocca-Volmerange; Buzzoni) by its spectral range (extreme ultraviolet to far-infrared), its complete coverage of the color-magnitude diagram, and its inclusion of observed near-infrared spectra out to 2.56 μm. Also, the spectra are distributed on the stellar evolutionary tracks using optical/near-infrared color calibrations, as an improvement over models that used a single color of the effective temperature of the stars alone.

The spectroscopic results obtained here confirm and extend the previous photometric predictions of the isochrone synthesis models while including the recent revision of evolutionary tracks for stars between 1.3 and 2.5 $M_\odot$ by their authors. Models with various time scales of star formation and a normal (Salpeter) initial mass function reproduce well the spectral and photometric properties from the ultraviolet to the near-infrared of nearby galaxies of various morphological types (from young irregular to older spiral and elliptical galaxies). We refine the stellar tracks to describe more accurately the evolution of hot planetary nebulae nuclei and white dwarfs and confirm in a self-consistent way the previous suggestion by Burstein et al. that these stars may account naturally for the far-ultraviolet radiation observed in "quiescent" early-type galaxies. The implications of the present models for the study of galaxy evolution are illustrated by the analysis of the redshift evolution of a few optical/near-infrared colors and spectral discontinuities for a representative range of model galaxies.

Subject headings: galaxies: luminosity function, mass function — galaxies: stellar content — stars: evolution — ultraviolet: galaxies

1. INTRODUCTION

This is the second of a series of papers in which we present "isochrone synthesis" as a natural and reliable approach to model the evolution of stellar populations in star clusters and galaxies (see Charlot & Bruzual 1991, hereafter CB91). The principle of this approach is to compute accurate isochrones in the color-magnitude diagram (CMD) for an instantaneous-burst stellar population (i.e., with no age dispersion) and to infer the properties of stellar populations with finite star formation rates by means of convolution integrals. The isochrones of the instantaneous-burst population are interpolated from a refined set of stellar evolutionary tracks, among which a large number of equivalent evolutionary phases have been especially identified. As a result, the distribution of stars of various masses and ages in the CMD evolves smoothly in time. Isochrone synthesis thereby overcomes the limitations of conventional models of population synthesis (Tinsley 1980; Bruzual 1983; Guiderdoni & Rocca-Volmerange 1987) that, because of their coarsely approximated isochrones, cannot be used reliably to study the evolution of rapid ($\ll$1 Gyr) starbursts. Models based on the fuel consumption theorem (Renzini 1981; Renzini & Buzzoni 1986; Buzzoni 1990) approximate reasonably well the distribution of stars in the CMD for an instantaneous starburst; however, they may underestimate the age assigned to stellar populations from the distribution of their light.

We assembled in CB91 a library of stellar evolutionary tracks suited for the isochrone synthesis approach. We improved over other existing libraries for solar metallicity (Bruzual 1983; Renzini & Buzzoni 1986; Guiderdoni & Rocca-Volmerange 1987) by limiting inhomogeneities in the input physics and by describing more accurately the late stages of stellar evolution. As a result, the *UBVRIJKL* photometric properties of the isochrone synthesis models were found to reproduce well the observations of nearby stellar populations. Short-burst models gave reasonable fits to the observed colors of young (0.01–4 Gyr) star clusters in the Large Magellanic Cloud (LMC), whereas longer time scales of star formation led to the observed colors of present-day galaxies in a full range of morphological types. The models also proved to reproduce well the contribution of bright asymptotic giant branch (AGB) stars to the bolometric light of star clusters as observed in the Magellanic Clouds. Recently, however, some tracks included in the library have been revised by their authors (Maeder & Meynet 1991; see also Schaller et al. 1992 and Bertelli, Bressan, & Chiosi 1992). While this revision does not affect at all our discussion in CB91 about the various approaches to population synthesis (conventional, fuel consumption therorem, or isochrone interpolation), it changes the details of the photometric results. This point is addressed in § 3.1 below. We conclude that, in fact, the revised tracks improve the previous success of the isochrone synthesis models at reproducing the

[1] Present address: Astronomy Department, University of California at Berkeley, Berkeley, CA 94720.

photometric properties of nearby stellar populations in a wide range of ages and star formation histories.

The main goal of this paper is to present the spectral energy distributions of stellar populations with solar metallicity computed with the isochrone synthesis algorithm. The spectra extend from 5 Å to 2.56 μm (plus four fluxes in the far-infrared corresponding to the four *IRAS* bands at 12, 30, 60, and 100 μm) and pertain exclusively to the stellar component. In § 2.1 below we briefly recall the characteristics of the library of stellar tracks assembled in CB91 and point out the recent revisions introduced by Maeder & Meynet (1991). Because the detail of the post-AGB evolution of low- and intermediate-mass stars plays an important role in the UV evolution of early-type galaxies (Burstein et al. 1988; Greggio & Renzini 1990; Magris & Bruzual 1992), we refine our treatment of these stars according to the prescription of Magris & Bruzual. In § 2.2. we assemble a complete library of stellar spectra to be assigned to stars on the tracks in the CMD. This library includes several improvements over earlier work. We analyze in § 3 the spectral evolution of a few isochrone synthesis models and compare our results with observations. In § 4 we present the evolution of a few colors and spectral discontinuities as a function of redshift for a representative range of model galaxies. Section 5 summarizes our results.

Copies of the spectrophotometric evolution of instantaneous-burst populations with different initial mass functions (IMFs) will be available in the near future from the Centre de Données Stellaires, 11 Rue de l'Université, F-67000 Strasbourg, France; and from the Astronomical Data Center, Code 633, NASA/Goddard Space Flight Center, Greenbelt, MD 20771, USA.

2. STELLAR INPUT

2.1. *Evolutionary Tracks*

The library of stellar evolutionary tracks used in the isochrone synthesis models has been compiled in CB91, to which we refer for details. The tracks are based largely on the recent computations of Maeder & Meynet (1989), who used a moderate efficiency of convective overshooting for stars more massive than about 1 $M_\odot$ (i.e., with lifetimes $\lesssim$10 Gyr). These authors, however, did not compute the evolution of low- and intermediate-mass stars through several important stages. We complemented their tracks in CB91 with tracks from other updated calculations, while limiting the inconsistencies in the stellar input physics between the different sets of tracks. Also, we determined semiempirically the evolution of low- and intermediate-mass stars through the luminous double-shell-burning regime at the end of the AGB, which is poorly understood by the theory. The resulting library of tracks presented in CB91 included the complete evolution of massive stars ($m \gtrsim 8\ M_\odot$) from the main sequence to the supernova explosion. The evolution of intermediate-mass stars with $2.5\ M_\odot \lesssim m \lesssim 7\ M_\odot$ was stopped at the end of the AGB phase.[2] For all stars less massive than 2.5 $M_\odot$, the evolution was followed up to the beginning of the white dwarf cooling sequence. We also added several unevolving stars with masses in the range $0.1\ M_\odot \leq m < 0.7\ M_\odot$ to ensure an accurate sampling of the main sequence at late ages.

Maeder & Meynet (1991) have since revised their tracks of stars with masses between 1.3 and 2.5 $M_\odot$, for which they had at first inadvertently overestimated the main-sequence lifetimes (see also Schaller et al. 1992). The revised lifetimes range from about 90% (2.5 $M_\odot$) to about 50% (1.3 $M_\odot$) of the original values. The duration of the post–main-sequence phases and the evolution of the effective temperature and luminosity of the stars, on the other hand, remain unchanged. We therefore include the new main-sequence lifetimes in our library of tracks.

Recently, Magris & Bruzual (1992) have refined the prescription adopted in CB91 of the post-AGB evolution of low- and intermediate-mass stars to study the far-UV properties of early-type galaxies. They added the post-AGB evolution of stars with initial masses in the range $2.5\ M_\odot \leq m \leq 7\ M_\odot$ using the tracks of Schönberner (1981, 1983). The connection between the CB91 AGB tracks in this mass range and the Schönberner tracks, however, requires the adoption of a relationship between the initial mass of a star and its core mass after ejection of the planetary nebula at the tip of the AGB. Because this relationship is still uncertain (see Weidemann 1990 for a review), Magris & Bruzual proposed two post-AGB extensions of the CB91 tracks based on the relationships of Iben & Truran (1978) and Weidemann (1987). For consistency with our assumptions on the AGB evolution in CB91, we adopt here the extension based on the Iben & Truran relationship. The final tracks include the evolution of all stars initially less massive than 7 $M_\odot$ as planetary nebulae (PNs), bare PN nuclei (PNNs, i.e., after dispersion of the envelope), and through the white dwarf cooling sequence.

The present library of stellar tracks therefore includes the evolution of stars in all mass ranges through all evolutionary phases from the main sequence to the remnant stage.

2.2. *Stellar Spectra*

We now assign spectral energy distributions to stars on the evolutionary tracks in the CMD. To cover all evolutionary stages, we must assemble a set of stellar spectra in a complete range of spectral types and luminosity classes. In the next paragraphs, we describe the different sets of data and the complementary models used to build this complete library of far-UV to far-IR spectra, for stars of solar metallicity. We then distribute the spectra on the evolutionary tracks in the CMD.

The spectra in the visible are taken from Gunn & Stryker (1983), who observed 175 stars of most spectral types and luminosity classes (3130 Å $\leq \lambda \leq$ 1.06 μm with 10 to 20 Å resolution). Persson (1987) supplemented the spectra of all but eight of these stars in the near-IR ($1.22 \leq \lambda \leq 2.56$ μm with 0.2 μm resolution) with data from the Kuiper Airborne Observatory (KAO) (see Strecker, Erickson, & Witteborn 1979 for stars of type earlier than M3 and Strecker, Erickson, & Witteborn 1989 for later-type stars).[3] We use here the resulting library of

[2] Stars in this mass range evolve through the hot post-AGB phase more rapidly than their envelope disperses, so that the UV radiation emitted when they are still bright is strongly attenuated (e.g., Spergel, Giuliani, & Knapp 1983). These stars, whose contribution to the optical/near-IR light is negligible, were neglected in CB91. Their treatment is refined in the next paragraphs.

[3] Persson tied together the KAO spectra with the Gunn & Stryker spectra using the $V-K$ color. For the hotter Gunn & Stryker stars, he inferred $V-K$ from $B-V$ via standard calibration relationships; for the cooler stars, he computed $V-I$ in the Cousins system from the Gunn & Stryker spectra and then converted it into Johnson $V-I$ and $V-K$ (after identification of the appropriate zero points and color terms). Interpolation in the grid of KAO spectra, sorted by $V-K$, then allows the assignment of an IR spectrum to any Gunn & Stryker star. Among the original Gunn & Stryker stars, six variables and two stars that did not have red enough KAO counterparts (Nos. 70 and 71) were left aside. No attempt was made to correct the Gunn & Stryker spectrophotometry for the declination effect pointed out by Taylor & Joner (1990). The σ per datum ($\sim$0.02) derived by these authors for the synthetic colors computed from the Gunn & Stryker scans is well within the allowance of population synthesis techniques.

visible/near-IR spectra that covers luminosity classes III, IV, V and all spectral types from O5 ($T_{\rm eff} \sim 40{,}000$ K) to M8 ($T_{\rm eff} \sim 2800$ K; material kindly made available to us by S. E. Persson). We complement each of the spectra with four far-IR fluxes at $\lambda = 12$, 25, 60, and 100 μm obtained either by direct identification of the Gunn & Stryker stars in the *Infrared Astronomical Satellite* Point Source Catalog (1985) or by using the fluxes of stars of the same spectral type scaled accordingly. For completeness we interpolate the flux at the effective wavelength of the L band ($\lambda = 3.4$ μm) in the spectra.

We use observations from the *International Ultraviolet Explorer* (*IUE*) to extend the spectra of the Gunn & Stryker (1983) stars in the range 1200 Å $\leq \lambda \leq$ 3240 Å (3 Å resolution; Bruzual 1983, Wu et al. 1983, Heck et al. 1984, Wu et al. 1991). Each star is assigned a UV spectrum according to its spectral type and luminosity class. The ultraviolet and visible spectra are then patched together using the 2980—4250 color measured by the *Orbiting Astronomical Observatory* (*OAO*; Code, Holm, & Bottemiller 1980). If the spectra are noisy in the overlapping region (from 3130 to 3240 Å), we use *OAO* spectra that cover the range 1200–3580 Å (Code & Meade 1979; Meade & Code 1980) to infer the shape of the spectrum between 3000 and 3600 Å. Because several types of stars in some luminosity classes are not included in published *IUE* libraries, we assign to these stars available *IUE* spectra of stars of the same spectral type and closest luminosity class (for instance, late-type dwarfs are assigned the UV spectra of red giants). Stars of type later than F5 ($T_{\rm eff} \lesssim 6500$ K) are assigned zero flux blueward of 2000 Å, as the signal-to-noise ratio in their *IUE* spectra drops substantially beyond this point. We extend the spectra of stars of earlier type in the range 240 Å $\leq \lambda <$ 1200 Å using Kurucz (1979) model atmospheres (with an average resolution of 20 Å).

The far-UV spectra obtained in this way do not cover all spectral types and luminosity classes in the tracks presented in § 2.1 (totaling 2455 stages for 32 stellar masses). In particular, stars with $T_{\rm eff} > 40{,}000$ K and supergiants are not represented (the only three supergiants observed by Gunn & Stryker 1983 were variable stars). To assign a spectral energy distribution to all stars on the tracks in the CMD, we proceed in three steps.

1. We adopt Kurucz (1979) model atmospheres ($\lambda \geq 240$ Å) for stars in all stages with 40,000 K $< T_{\rm eff} \leq$ 50,000 K. Stars of higher $T_{\rm eff}$ (massive stars burning carbon in their core, or hot PNNs) are assigned pure blackbody spectra at all wavelengths $\lambda \geq 5$ Å due to the lack of refined models or observations.

2. To assign a spectrum to cool stars, we first select a set of the late-K and M stars (dwarfs and giants) in the Gunn & Stryker atlas for which the computed $U-V$, $B-V$, $V-R$, $V-I$, $V-J$, $V-H$, and $V-K$ colors match the color calibrations for K and M stars of Johnson (1966) and Bessel & Brett (1988).[4] Each of the selected spectra is assigned a value of $T_{\rm eff}$ according to the calibration of Johnson (1966) for the main-sequence stars and Ridgway et al. (1980) for the giant stars. Every star in the evolutionary tracks with $T_{\rm eff} < 4930$ K (giants) or $T_{\rm eff} < 5240$ K (main sequence) is then assigned a spectrum inferred from this set by interpolating linearly in log $T_{\rm eff}$ between the two bracketing spectra available for the same luminosity class. Because of the lack of data, M supergiants are assigned the spectra of M giants of the same $T_{\rm eff}$.

3. We select spectral energy distributions for stars with $3700 \leq T_{\rm eff} \leq 40{,}000$ K from the observed spectra compiled above as follows. As in CB91, we use standard calibrations (Böhm-Vitense 1972; Flower 1977; Buser & Kurucz 1978) to transform the tracks from the (log $T_{\rm eff}$, log L)-diagram to the (V, $B-V$)-diagram. We use Johnson's (1966) calibration of the *UBVRIJKL* photometric system to obtain the $U-V$, $V-R$, $V-I$, $V-J$, and $V-K$ colors corresponding to the $B-V$ color and luminosity class for each point along the tracks.[4] The spectrum assigned to a given evolutionary stage on a track is then the one with closest optical/infrared colors in the library. In practice, we first select the available spectrum that provides the smallest sum of squared residuals for the six colors above. We then also investigate linear combinations of a few spectra of close types, with the constraint of positive weights (using the "nonnegative least-squares" algorithm of Lawson & Hanson 1974). In only 5% of the cases, however, does such a combination of two or three spectra improve the residuals obtained with a single spectrum significantly and therefore become adopted. We then scale the selected spectrum by computing with equation (6) of Code et al. (1976) the absolute V flux corresponding to the calibrated bolometric correction at the point in the CMD. Since we do not have spectra for supergiants, we approximate them by spectra of main-sequence stars of the same $T_{\rm eff}$. Even though some of the 167 Gunn & Stryker stars may have nonsolar metallicities, the selection criterion imposed above ensures that only stars with colors resembling those of solar metallicity stars are chosen. This procedure was checked to be efficient, since no star with deviant colors was selected. The final selection includes 103 of the stars in the Gunn & Stryker atlas.

For completeness, we include the reddening of stars evolving through the planetary nebula phase (i.e., during the first $\sim$30,000 yr on the post-AGB; e.g., Schönberner 1986). Here we adopt the Galactic extinction law of Savage & Mathis (1979) and the mean optical depth for PNs, 1.9×10^{-3} at $\lambda = 30$ μm, inferrred from Table VIII-1 of Pottasch (1984). We also calibrate separately the spectra of stars with circumstellar shells undergoing thermal pulses on the tip of the AGB using the colors of Mira Ceti and IK Tau (see CB91). The spectra of all stars on the tracks are assigned a uniform wavelength scale, 1206 points from 5 Å to 100 μm, with a resolution in the various spectral ranges imposed by the original data or model.

2.3. *Comparison with Earlier Models*

We discussed in CB91 the improvements introduced by the library of stellar tracks described above over earlier models of population synthesis (Bruzual 1983; Renzini & Buzzoni 1986; Guiderdoni & Rocca-Volmerange 1987; Buzzoni 1990). The revision of the post-AGB evolution of low- and intermediate-mass stars constitutes another amelioration, since these stars have not been accounted for consistently with their evolution in earlier stages (main sequence, giant branch, etc.) in previous models.

The stellar spectra also present several improvements over earlier work. The pioneer model of Gunn, Stryker, & Tinsley (1981) included spectra only in the visible from the Gunn & Stryker (1983) library. Bruzual (1983) used lower resolution

[4] We adopt the bandpass response functions of Buser (1978) for the *UBV* filters and of Johnson (1965) for the *RIJ* filters. The bandpass of the K filter in use at Palomar Observatory was kindly provided to us by S. E. Persson. The H bandpass is from Bessel & Brett (1988). The zero points of all colors are calibrated on the model atmosphere of α Lyr by Kurucz (1979). Multiple tests performed on stellar and galaxy spectra show that the observed colors are recovered at the level of a few hundredths of a magnitude.

spectra in the visible (Straižys & Sviderskiene 1972) and a less complete set of *IUE* spectra than adopted here in the UV (Code & Meade 1979; Bruzual 1983). Guiderdoni & Rocca-Volmerange also had a coarser library of *IUE* spectra (from Wu et al. 1983), but they improved the spectra in the visible over Bruzual (1983) by implementing the Gunn & Stryker (1983) data in their model. Neither Bruzual (1983) nor Guiderdoni & Rocca-Volmerange (1987) complemented the spectra redward of 1 μm in their models, and they accounted for the near-IR light only by means of broad-band fluxes. Bruzual (1987) substituted the Gunn & Stryker spectra for the Straižys & Sviderskiene spectra in his earlier model and included the near-IR spectra of Persson (1987). The evolutionary tracks, however, were kept the same in this later version of his model. Buzzoni (1990) took a different approach in a model based entirely on theoretical stellar atmospheres by Kurucz (1979) and Bell & Gustafsson (1978) that extend from 229 Å to 20 μm. As Buzzoni points out, the main advantage of this approach is that the bolometric correction of stars on the tracks does not have to be inferred from empirical relationships. The main drawback is that it probably underestimates the blanketing effect, since all chemical elements cannot be accounted for in the model atmospheres.

The procedure adopted here to assign a stellar spectrum from the library to different locations on the evolutionary tracks also is improved over earlier work. Bruzual (1983, 1987) and Guiderdoni & Rocca-Volmerange (1987) assigned to a given evolutionary stage on the tracks the available spectrum of the same luminosity class with the closest $B-V$ color or $T_{\rm eff}$. However, stars with the same $B-V$ color or $T_{\rm eff}$ may have different spectra, even if they belong to the same luminosity class (e.g., stars along the red giant branch). Spectral assignments relying on one color only may therefore be misleading. The approach proposed here, based on matching calibrated colors in the full *UBVRIJK* photometric range, is more reliable and allows us to exploit fully the better quality of the new libraries of tracks and spectra, especially in the near-IR. The model of Buzzoni (1990) of course overcomes the problems of selecting observed spectra, since model atmospheres can be computed at arbitrary temperatures and luminosities. However, because of the limitations of published material, Buzzoni still had to extrapolate model atmospheres for stars cooler than 4000 K and to assume a pure blackbody law for stars hotter than 50,000 K.

3. ISOCHRONE SYNTHESIS MODELS

We use here the libraries of stellar tracks and stellar spectra presented in the previous section to compute the evolution of the spectral energy distribution $f_\lambda(t)$ of an instantaneous-burst stellar population. The integrated spectrum $F_\lambda(t)$ of a stellar population with arbitrary star formation rate $\Psi(t)$ can then be obtained with the convolution integral

$$F_\lambda(t) = \int_0^t \Psi(t-\tau) f_\lambda(\tau) d\tau \ , \qquad (1)$$

provided that the IMF does not evolve in time. We compute $f_\lambda(t)$ for the instantaneous-burst population by adding up the spectra of the stars on the isochrone at age t. The isochrone is interpolated from the stellar evolutionary tracks, and the number of stars of various masses in various evolutionary stages are calculated from the IMF, as described in CB91. The spectrum to be attributed to each type of star is then interpolated in a similar way.

Unless otherwise indicated, the models presented in the remainder of this paper have a Salpeter (1955) IMF with lower and upper cutoffs $m_L = 0.1\ M_\odot$ and $m_U = 125\ M_\odot$. The total mass in stars of the model galaxies is 1 $M_\odot$.[5] Typically, spectral energy distributions are computed at 220 (unequally spaced) model ages from about 1×10^5 to 2×10^{10} yr. Each spectrum extends from 5 Å to 100 μm (1206 wavelength points in total) with a resolution that depends on the spectral range (see § 2.2). We point out that the photometric properties of model galaxies are computed here by convolving their spectral energy distributions with the response functions of standard filters (spectroscopic model). This differs from our approach in CB91, where we did not have spectral information on the model galaxies and inferred their integrated photometric flux in a given wave band by adding up the photometric fluxes of individual stars in that wave band (purely photometric model). In what follows, we shall not discuss the far-IR properties of the models, because comparisons with real galaxies would require that radiation by dust grains in the interstellar medium be included.

3.1. *Comparison with CB91*

There are three main sources of possible discrepancies between the predictions of the present model and those of the model presented in CB91: (1) the reduction of the main-sequence lifetimes of some stars in the library; (2) the revision of the late post-AGB phase; and (3) the fact that the photometric fluxes are now computed from the spectral energy distributions $F_\lambda(t)$, whereas in CB91 we summed up directly the photometric contributions of individual stars. None of these differences affects our analysis in CB91 of the different approaches to computing the isochrones in the theoretical Hertzsprung-Russell diagram from an arbitrary set of tracks. Also, the evaluation of the uncertainties introduced by models based on the fuel consumption theorem with respect to the isochrone synthesis method (Figs. 3*a* and 3*b* of CB91) remains valid, since it was based on a common library of stellar evolutionary tracks. Furthermore, the refinement of the hot post-AGB and the addition of the white dwarf cooling sequence have a noticeable effect only in the UV; thus they do not affect significantly the *UBVRIJKL* photometric predictions of CB91.

In Figure 1 we show the evolution of the V-magnitude and $U-B$, $B-V$, and $V-K$ colors of a 10^7 yr burst population computed with the present spectroscopic model (*solid lines*) and with the purely photometric model of CB91 using the old (*dashed line*) and new (*dot-dash line*) prescriptions of the main-sequence lifetimes for stars between 1.3 $M_\odot$ (turnoff age $\sim$4.4 Gyr) and 2.5 $M_\odot$ (turnoff age $\sim$0.64 Gyr). The good agreement between the spectroscopic model and the photometric model with revised tracks confirms that the library of stellar spectra has good coverage of the spectral types defining the *UBVRIJKL* photometric system (Johnson 1966). As expected, the reduction of the main-sequence lifetimes leads to redder colors at ages between 0.6 and 4 Gyr, which in fact improves the fit of the observed colors of LMC clusters (*filled squares*) in all wave bands (see caption for source). However, the present

[5] The model galaxies in CB91 were inadvertently assigned a mass of 0.354 $M_\odot$ instead of 1 $M_\odot$, resulting in magnitudes 1.128 mag fainter.

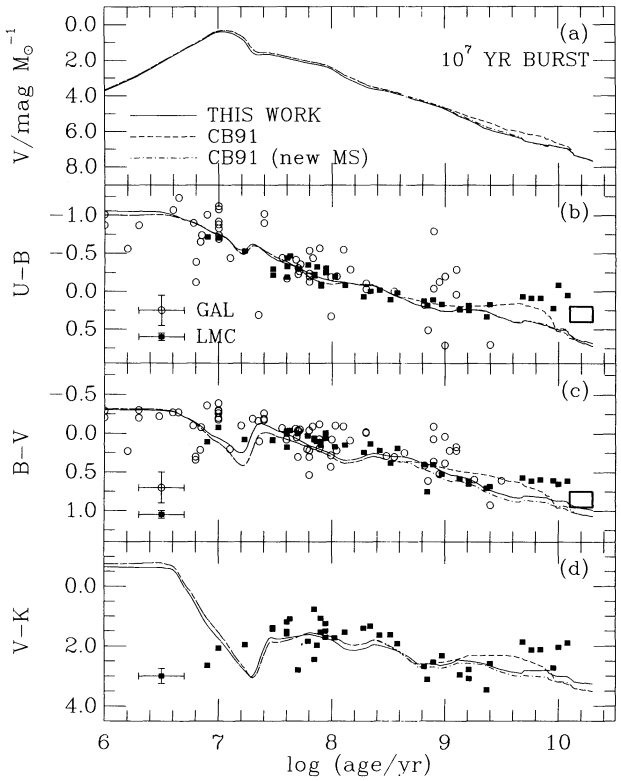

FIG. 1.—Photometric evolution of a 10^7 yr burst population computed with the present model of spectral evolution (*solid lines*) and with the purely photometric model of CB91 for the old (*dashed lines*) and new (*dot-dashed line*) prescriptions of the main-sequence lifetimes of stars from 1.3 to 2.5 $M_\odot$. (*a*) V-magnitude; (*b*) $U-B$ color; (*c*) $B-V$ color; (*d*) $V-K$ color. The scale of the V-magnitude corresponds to a stellar population of total mass 1 $M_\odot$. The filled squares are for a sample of LMC clusters with infrared photometry by Persson et al. (1983), *UBV* photometry by van den Bergh (1981), and ages by Elson & Fall (1988). The open circles are for the sample of Galactic open clusters by Pandey et al. (1989). The heavy boxes indicate the expected colors of Galactic globular clusters of solar metallicity (see text). All observed colors are corrected for reddening. Typical error bars are indicated on the figure.

models for solar abundances cannot fit the blue colors of the older, more metal-poor clusters (CB91 and references therein). Figure 1 also includes the $U-B$ and $B-V$ colors of a sample of Galactic open clusters (Pandey et al. 1989; *open circles*), whose metallicities should be closer to solar than those of the LMC clusters (e.g., Zinn 1986). Even though the scatter in the observed colors is significantly larger than for the LMC clusters, the model is consistent with the data at all ages. Open clusters, nonetheless, are rarely older than a few billion years. A good test for the models at older ages is to compare them with the colors of halo globular clusters with solar metallicity. The mean age of Galactic globulars is still very uncertain, about 16 ± 3.5 Gyr (e.g., Buonanno 1986), but their optical colors appear to correlate with metallicity. Simple linear regressions between the $U-B$ and $B-V$ colors of 41 Galactic globulars (Racine 1973) for which measurements of [Fe/H] are available (Sandage 1982) yield $U-B \approx 0.30 + 0.13$[Fe/H] and $B-V \approx 0.84 + 0.10$[Fe/H], with a mean dispersion of 0.1 mag. In Figure 1 we have used the zero points of these relations to indicate the mean colors of Galactic globulars with solar metallicity (*heavy boxes*). These are redder than the colors of metal-poor LMC clusters, but the $U-B$ color is still slightly bluer than the models. In fact, the present models reproduce better the colors of old elliptical galaxies, which have on average redder colors than those adopted here for globular clusters (§ 3.4).

We have also checked that the reduction of the main-sequence lifetimes for stars between 1.3 and 2.5 $M_\odot$ does not alter the main results of our comparison of the models in CB91 (their Fig. 11) with the observed colors of present-day galaxies of various Hubble types. The reason is that the data were fitted at ages $\lesssim 1$ Gyr (Im) or $\gtrsim 13$ Gyr (earlier types), when stars in this mass range do not dominate the photometric properties for exponentially decreasing (or constant) star formation rates. However, the exact matching of the new model colors to the colors of present-day galaxies is sensitive to the blueing of the $U-V$ and $V-K$ colors at late ages (Fig. 1). This leads to slightly younger ages than those derived by CB91 (see also § 3.4 below).

The most significant differences between the present models and those of CB91 occur when stars between 1.3 and 2.5 $M_\odot$ dominate the photometric properties of the population, e.g., from about 1 to 4 Gyr for an instantaneous starburst. In Figure 2 we show the contributions of stars in different evolutionary stages to the integrated light of an instantaneous-burst population (bolometric and in various spectral ranges) as predicted by the present models. As expected, after about 1 Gyr the contribution of main-sequence stars is much less in all wave bands than indicated in the analogous Figure 8 of CB91 (see also § 3.3 below). As a result, the AGB contribution to the bolometric light at 1×10^9 yr is a few percent more than the value indicated in Figure 4 of CB91, which improves the fit of the observed contribution in the Magellanic Cloud clusters. We also show in Figure 2 the fractional contributions of the various star groups to the fluxes at 1400 and 2200 Å. At these wavelengths, one observes a bimodal distribution of the light between main-sequence stars and PNNs. We note that the PNN contribution rises earlier at 1400 Å than at 2200 Å because stars of higher masses produce hotter nuclei. The predicted contribution of white dwarfs is significant only at 1400 Å and never exceeds 10%.

Hence, we conclude that the revised library of stellar tracks confirms and even improves the comparisons of the CB91 photometric models with observations, and that the spectral library introduced in § 2.2 has adequate coverage of the color-magnitude diagram.

3.2. *Color-Magnitude Diagrams*

To establish the accuracy of the magnitude scale of the models, we must complement the fits of the integrated colors of star clusters with comparisons between predicted isochrones and observed color-magnitude diagrams. This is shown in Figure 3, where we compare the models against various color-magnitude diagrams of two of the best-studied clusters with nearly solar metallicity, M67 ([Fe/H] ≈ 0.01) and the Hyades ([Fe/H] ≈ 0.15). The model isochrones, corresponding to an instantaneous starburst, were computed by convolving the stellar spectra with the response functions of the filters used in the observations. We have adopted a distance modulus of 9.5 mag and a color excess $E(B-V) = 0.06$ mag for M67 (Janes 1985), and a distance modulus of 3.4 mag (Peterson & Solensky 1988) for the Hyades [$E(B-V) \approx 0$]. The various estimates of the ages of these clusters in the literature roughly agree on about 4–4.3 Gyr for M67 and about 0.5–0.8 Gyr for the Hyades.

Figures 3*a*–3*d* show that the model reproduces reasonably well the observed distribution of stars in M67 in the *UBVRI* photometric bands at an age of 4 Gyr. In detail, however, there

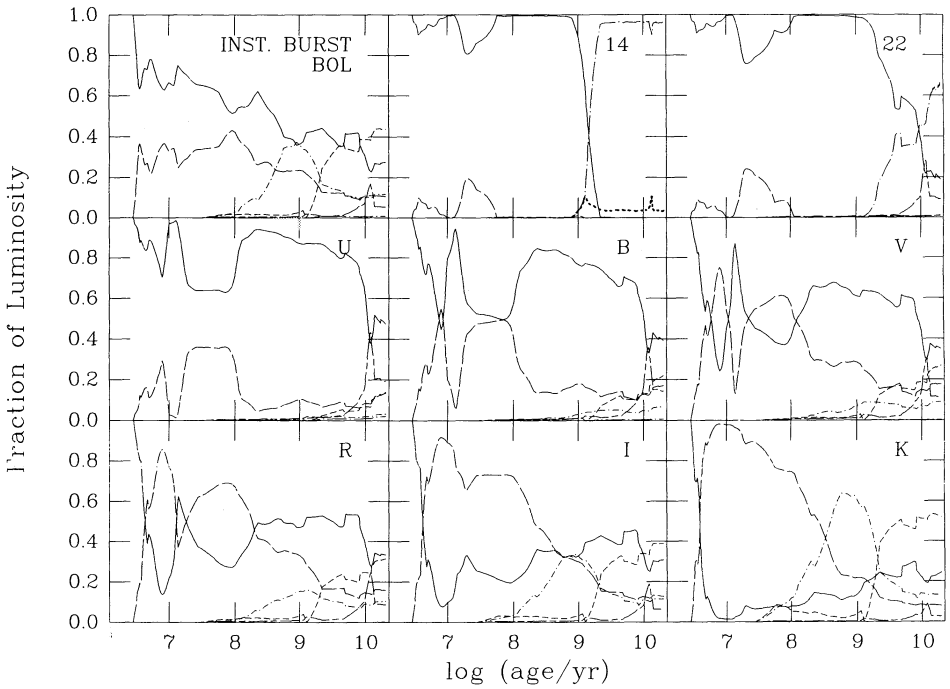

FIG. 2.—Fractional contribution to the integrated light of an instantaneous-burst population by the various stellar evolutionary stages, as predicted by the present model of spectral evolution (isochrone synthesis). The nine panels indicate the contributions to the bolometric light, to the fluxes at 1400 and 2200 Å, and to the broad-band *UBVRIK* fluxes. In each panel the different curves correspond to the following stellar evolutionary stages (acronyms defined in § 3.5): main sequence (*solid line*), SGB (*short-dash–long-dash line*), RGB (*dashed line*), CHeB (*long-dashed line*), AGB (*dot–short dash line*), PNN (*dot–long dash line*), and WD (*short-dashed line*).

are some discrepancies. In particular, the transition between the stellar tracks of Maeder & Meynet (1989, 1991) and those with higher efficiency of convective overshooting by Chiosi (1990; see CB91) causes the isochrone on the main sequence to become slightly bluer than the data around $V \gtrsim 15$. While this discrepancy is less than 0.1 mag in all colors, no updated stellar model appears to be available at present that could be used to describe the evolution of low-mass stars more consistently with that of higher mass stars (CB91). The stars on the blueward extension of the well-defined main-sequence turnoff are "blue stragglers" that have been studied in detail previously (e.g., Gilliland et al. 1991). Figures 3*e* and 3*f* show similarly that the models reproduce acceptably well the main-sequence and core He-burning loci of the Hyades cluster at an age of 0.6 Gyr (note again the slight blueing of the main sequence at faint magnitudes). We conclude that even though some discrepancies are found, the agreement between the predicted isochrones and the color-magnitude diagrams of standard star clusters may be regarded as satisfactory.

3.3. *Spectral Evolution*

Figure 4*a* shows the spectral evolution of an instantaneous-burst population, $f_\lambda(t)$ in units of $L_\odot$ Å^{-1} $M_\odot^{-1}$, and is best understood when analyzed simultaneously with Figure 2. At age 1×10^6 yr, the spectrum is almost completely dominated by blue main-sequence stars. After 1×10^7 yr, the most massive stars have evolved off the main sequence and become red supergiants, making the UV light drop and the near-infrared light rise. From a few times 10^8 yr to $\gtrsim 1 \times 10^9$ yr, the AGB stars maintain a high near-infrared luminosity, and the UV light continues to drop as the turnoff mass decreases on the main sequence. After a few times 10^9 yr, the red giant branch takes over the production of the near-infrared light. The rise in the far-UV after 4–10 Gyr is produced by low-mass stars in their post-AGB evolution and resembles the "UV-rising" branch observed in early-type galaxies (Burstein et al. 1988; Greggio & Renzini 1990; see § 3.4 below). Furthermore, hot post-AGB stars make the amplitude of the 912 Å discontinuity decrease once their envelope has dissipated.

We have also computed the spectral evolution of stellar populations with longer time scales of star formation. These are shown in Figures 4*b*–4*d* for exponentially decreasing star formation rates,

$$\Psi(t) = \tau^{-1} \exp(-t/\tau), \quad (2)$$

of time scales $\tau = 3$ Gyr, 7 Gyr, and ∞ (constant star formation). The UV-to-optical spectrum remains roughly constant during the main episode of star formation because of the continuous input of young massive stars, but the near-infrared light rises as evolved stars accumulate. When star formation drops, the spectral characteristics at various wavelengths are determined by stars in advanced stages of stellar evolution, as can be inferred from Figure 4*a*.

3.4. *Comparisons with Observed Spectra*

We now test the isochrone synthesis models against spectral energy distributions representative of nearby galaxies of different morphological types. We refer to these as "observed" spectral energy distributions, even though they were assembled from different sets of observations covering different spectral ranges (due to obvious observational limitations). We investigate various star formation rates and select in each case the model age providing the best fit to an observed spectrum by

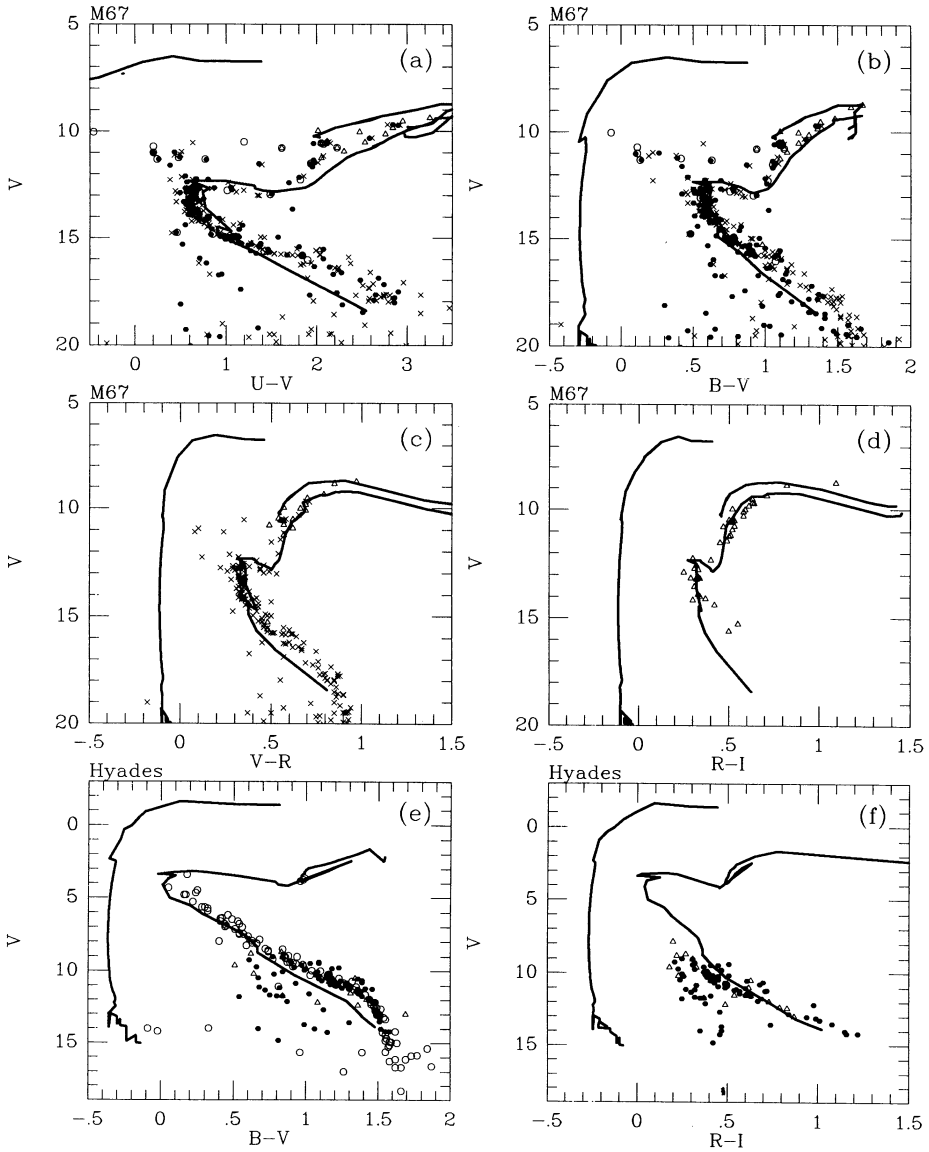

FIG. 3.—Comparison of model isochrones for an instantaneous starburst with the color-magnitude diagrams of standard star clusters. (*a–d*) M67 vs. the 4 Gyr isochrone in various colors. The data are from Eggen & Sandage (1964; *open circles*), Racine (1971; *filled circles*), Janes & Smith (1984; *triangles*), and Gilliland et al. (1991; *crosses*); (*e, f*) Hyades vs. 0.6 Gyr isochrone in two colors. The data are from Upgren (1974; *triangles*), Upgren & Weis (1977; *filled circles*), and Micela et al. (1988; *open circles*). The model isochrones, which include distance modulus and reddening, were computed from the stellar spectra using the same filters as for the observations. See text for discussion.

minimizing the following sum of squared residuals

$$R_k^2 = \sum_{i=1}^{N} [\Delta \log F_{\lambda_i}]^2 = \sum_{i=1}^{N} [\log F_\lambda^{\rm obs}(\lambda_i) - \log F_\lambda(\lambda_i, t_k)]^2 \ , \tag{3}$$

where λ_i, for $i = 1$ to N, represents the wavelength scale of the observed spectrum, and t_k is the model age at which R_k^2 is computed.

In Figure 5 we compare the spectral energy distribution of a 1 Gyr burst model and that of an "average" quiescent elliptical galaxy with a UV spectrum of the type of NGC 4472 (Burstein et al. 1988). The model is shown at the best-fitting age of 13.5 Gyr. The observed spectrum between 3000 Å and 1.06 μm is an average over five first-ranked (radio-quiet) elliptical galaxies by Yee & Oke (1978; kindly provided to us by J. B. Oke). The UV spectrum from 1250 to 3000 Å is a compilation of the spectra of the five early-type galaxies NGC 4472, NGC 3115, NGC 224, NGC 4374, and NGC 1404 classified as quiescent by Burstein et al. (1988). We added the three near-infrared fluxes in such a way that the resulting spectrum has the mean $\langle V-K\rangle = 3.20$, $\langle J-K\rangle = 0.90$, and $\langle J-H\rangle = 0.70$ colors of a standard elliptical galaxy (Aaronson 1978; Persson et al. 1992).[6] The vertical scale of the observed spectrum in Figure 5*a* was adjusted by making the algebraic sum of residuals, $\sum_{i=1}^{N} \Delta \log F_{\lambda_i}$, vanish (Fig. 5*b*).

For this type of galaxy the fit is very good over the whole spectral range, and no systematic trend is observed in the

[6] The spectrum compiled here has a synthetic $B-V$ color of 0.89, i.e., slightly bluer than the average $\langle B-V\rangle = 0.92$ for elliptical galaxies (Persson et al. 1992). The best-fitting age of the model would be larger for a redder $B-V$.

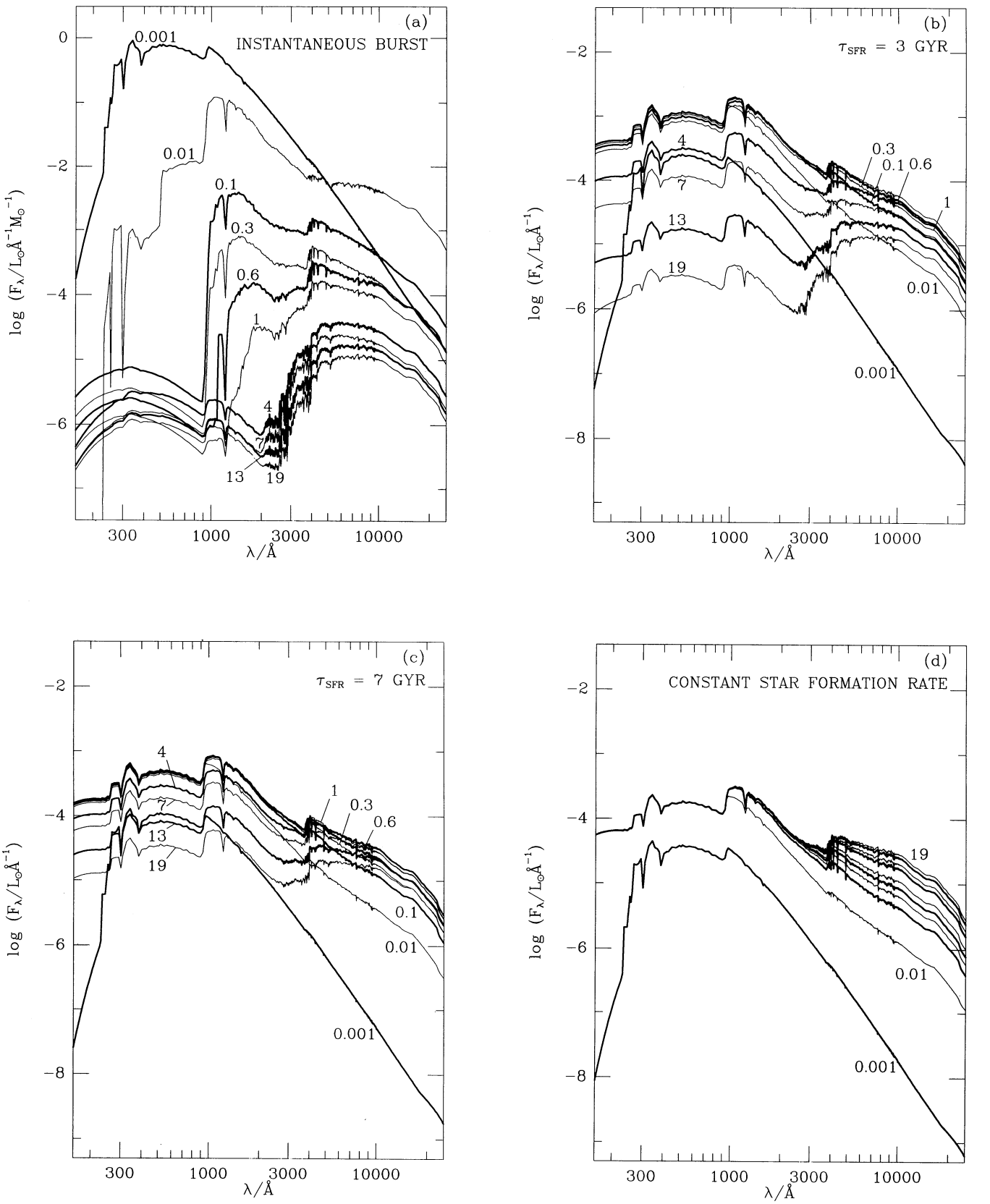

FIG. 4.—Spectral evolution of stellar populations with different star formation rates as predicted by the isochrone synthesis model: (*a*) instantaneous starburst; (*b*) eq. (2) with $\tau = 3$ Gyr; (*c*) eq. (2) with $\tau = 7$ Gyr; and (*d*) constant star formation. In each case, the age (in Gyr) is indicated next to the spectra. Thick lines and thin lines have been used alternatively for clarity. All models have the Salpeter IMF.

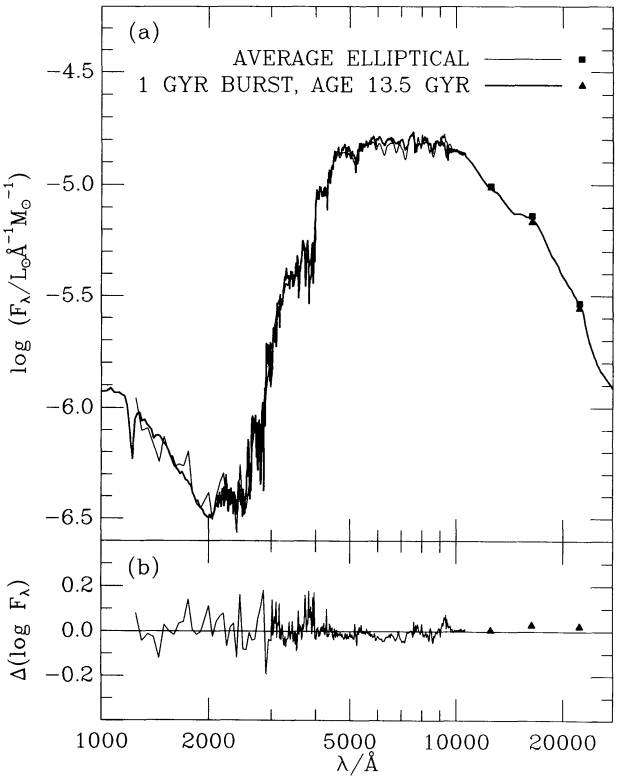

FIG. 5.—(*a*) Comparison of the 1 Gyr burst model at age 13.5 Gyr (*thick line and triangles*) with the average spectrum of an observed elliptical galaxy (*thin line and squares*; see text for source). The squares and the triangles correspond to the fluxes at the effective wavelengths of the *J*, *H*, and *K* bands inferred by dividing broad-band fluxes by the respective bandwidths. (*b*) Residuals of the comparison in (*a*). The model has a Salpeter IMF.

behavior of the residuals with wavelength. The main stellar absorption features in the observed spectrum and the amplitude of the 4000 Å break are well reproduced by the model. Together with the good agreement in the UV and the near-IR, this constitutes an improvement over earlier detailed population synthesis models (Bruzual 1983; Guiderdoni & Rocca-Volmerange 1987). We attribute this result to the more accurate treatment of the late stages of stellar evolution, whose adequate sampling is also ensured by the isochrone synthesis approach, and to the refined spectral calibration of the model stars. The model fits better the spectrum of the elliptical galaxy considered here than the mean colors of globular clusters (Fig. 1), because elliptical galaxies appear to have on average redder colors than globular clusters with solar metallicity (§ 3.1). The UV-rising branch of the elliptical galaxy in Figure 5 is explained as a natural consequence of late stellar evolution. This confirms the suggestion made by Burstein et al. (1988) on the basis of a more ad hoc model, whereby they questioned the conclusions of models without post-AGB stars that required recent star formation (Bruzual 1983; Guiderdoni & Rocca-Volmerange 1987). At later ages, the UV-rising branch remains constant in the model, but the $B-V$ color reddens, making the fit slightly worse. We have obtained similar fits to the one shown in Figure 5 for the optical spectra of the early-type galaxies NGC 3379, NGC 4472, or NGC 4889 published by Kennicutt (1992; see Fig. 7*a*). However, these observed spectra do not extend as far into the infrared as the Yee & Oke spectrum shown here. We also note that the model of Figure 5 appears to overestimate slightly the flux in the wavelength range 6000 Å $\lesssim \lambda \lesssim$ 7000 Å with respect to the average elliptical galaxy. This should not be interpreted as a general limitation of the models, since the spectral fit of NGC 3379 shown below in Figure 7*a* is excellent at these wavelengths. Such differences in the observed spectra of elliptical galaxies most likely reflect different metallicity distributions among their stellar populations.

It is interesting to examine why the present models based on solar metallicity stellar properties can fit the spectra of elliptical galaxies which, like NGC 4472, show stellar components of higher metallicities (Davies et al. 1987; Worthey, Faber, & Gonzalez 1992). Some insight may be gained here by computing the Mg_2 index (Faber et al. 1985) and the 4000 Å break (Bruzual 1983) of the elliptical galaxies in the Kennicutt (1992) sample. For the galaxies NGC 3379, NGC 4472, and NGC 4889 we find Mg_2 indices of 0.23, 0.25, and 0.27, and 4000 Å breaks of 2.1, 2.0, and 2.2, respectively. For comparison, the Mg_2 index and 4000 Å break of the best-fitting model of Figure 5 are 0.23 and 2.3, respectively. These Mg_2 indices are characteristic of galaxies with about solar metallicity (Burstein et al. 1988). Also, the values quoted above for the 4000 Å breaks are significantly lower than the values 2.4–2.5 found in galaxies of presumably higher metallicities (see § 4.2 below). Burstein et al., on the other hand, report Mg_2 indices of 0.329 and 0.331 for NGC 3379 and NGC 4472. This disagreement with the values computed above comes most likely from the fact that Kennicutt performed large-aperture observations (a few arcmin^2), while Burstein et al. adopted the spectroscopic data of Davies et al., who sampled small areas near the centers of the galaxies (a few arcsec^2) and identified large populations of stars with high metallicities (see also Worthey et al.). Hence, the population seen through the large-aperture observations of Kennicutt must have on average near-solar metallicity. This would explain why the present models can reproduce the spectra of these galaxies.

Elliptical galaxies can have steeper UV-rising branches than the one shown in Figure 5 (Burstein et al. 1988). We found that a 1 Gyr burst model fails at all ages to reproduce the UV excess of the four quiescent galaxies NGC 1399, NGC 4552, NGC 4649, and NGC 1407 with the bluest (1550 $-$ V) colors in the sample of Burstein et al. A possible interpretation in the framework of the present models with solar metallicity is that a small amount of residual star formation of the order of 0.03 $M_\odot$ yr^{-1} has been taking place in these galaxies after an initial burst of 100 $M_\odot$ yr^{-1} lasting for 1 Gyr (Magris & Bruzual 1991, 1992; Bruzual 1991), in agreement with Bertelli, Chiosi, & Bertola (1989). More exotic interpretations have been discussed by Greggio & Renzini (1990). The UV spectrum of the galaxy M32 in the Burstein et al. sample can be understood by invoking two events of star formation: an initial burst of duration 1 Gyr and a second burst of the same duration occurring 4 Gyr ago. Each of these bursts would encompass half of the galaxy mass seen through the *IUE* aperture (Magris & Bruzual 1992; Bruzual 1991). This result is in accord with O'Connell (1986) and Bertelli et al. (1989), but has been questioned by Greggio & Renzini (1990).

In Figure 6 we compare a model of constant star formation rate with the observed spectral energy distribution of the irregular galaxy NGC 4449. The best-fitting age in this case is 1 Gyr. The observed spectrum from 1250 Å to 2.2 μm was assembled from *IUE*, optical, and near-IR data by Ellis & Bruzual (1983). The residuals between model and data are very

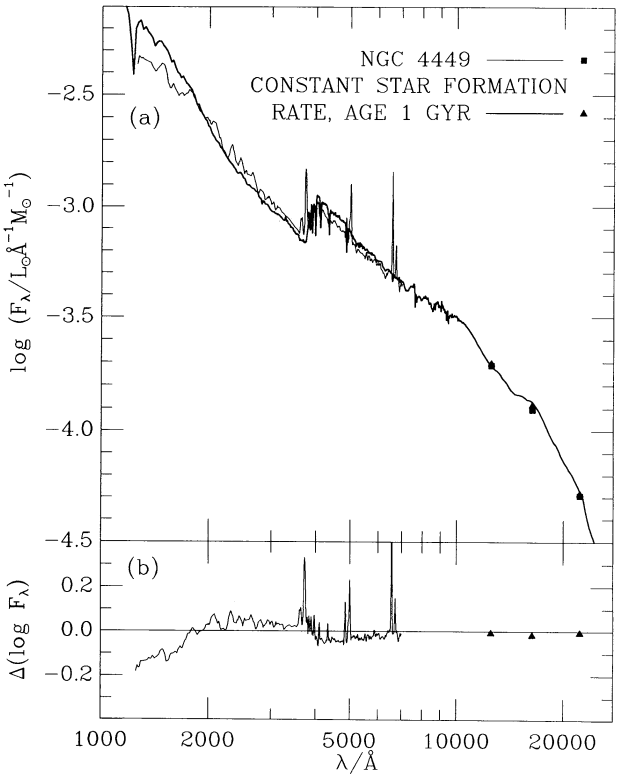

FIG. 6.—Comparison of a model with constant rate of star formation at age 1 Gyr (*thick line and triangles*) with the blue irregular NGC 4449 (*thin line and squares*; see text for source). The squares and triangles have the same meanings as in Fig. 5. (*b*) Residuals of the comparison in (*a*). The model has a Salpeter IMF.

small, except blueward of 1500 Å, where the model shows an excess of UV radiation (the model cannot reproduce the observed emission lines, since we did not consider a nebular component). Reducing the proportion of massive stars in the IMF would help, but the 4000 Å break would then rise in the model and make the fit worse in the optical. An alternative explanation is that internal dust in the galaxy extinguishes some of the ultraviolet light.

Since the isochrone synthesis model reproduces well the observed spectra of old elliptical galaxies (dominated by low-mass stars) and of young irregulars (dominated by massive stars), we expect it to reproduce also the spectra of galaxies with arbitrary star formation rates. To verify this contention, we now compare models with different time scales of star formation with the characteristic spectra of galaxies of various morphological types obtained by Kennicutt (1992). We compute isochrone synthesis models with exponentially decreasing star formation rates (eq. [2]) for time scales of star formation τ ranging from 1 to 7 Gyr. Such models were shown in CB91 to reproduce well the optical and near-IR colors of bright galaxies of various morphological types. We present four model spectra in Figure 7 found to give good agreement with the four representative spectra of NGC 3379 (E0), NGC 3147 (Sb), NGC 5248 (Sbc), and NGC 6181 (Sc) obtained by Kennicutt (1992) in the range 3600–8000 Å. As expected, models with increasing time scales of star formation can reproduce the spectra of galaxies from early to late morphological types. Again, the main absorption features and the 4000 Å breaks of the models match the observations reasonably well. We have also checked that the models selected here have the typical $U-V$ and $V-K$ colors observed in E, Sb, Sbc, and Sc galaxies (§ 3.1 above and CB91). This suggests that the spectral fits are likely to extend down into the near-infrared.

The best-fitting ages determined in the previous comparison of the models with observed spectra are, in fact, very loosely constrained. To illustrate this, we show in Figure 8 the evolu-

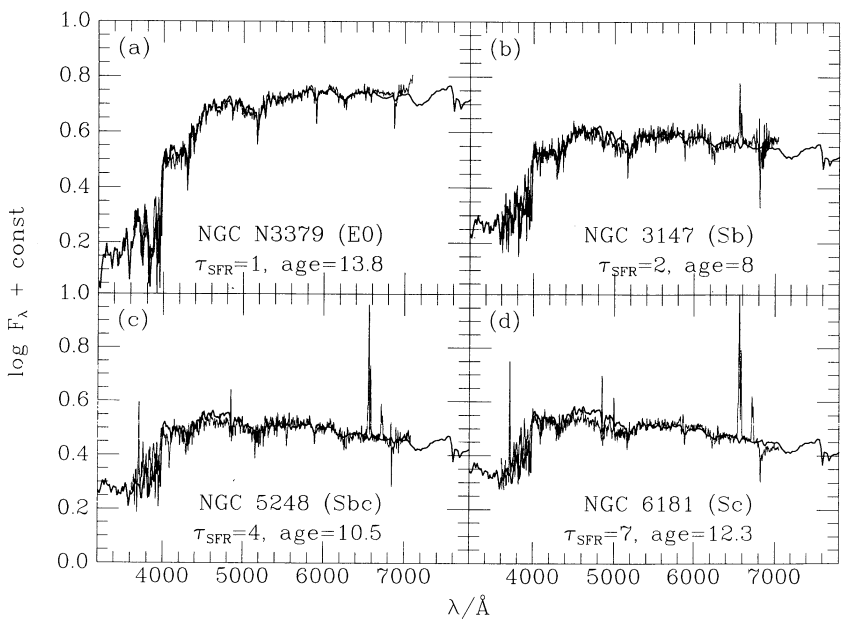

FIG. 7.—Comparison of models with different time scales of star formation (*thick lines*) with the typical spectra of galaxies of various morphological types (*thin lines*; from Kennicutt 1992). (*a*) NGC 3379 (E0); (*b*) NGC 3147 (Sb); (*c*) NGC 5248 (Sbc); (*d*) NGC 6181 (Sc). The time scale of star formation (eq. [2]) and the age of the model are indicated (in Gyr) in each panel (see text for discussion). All models have a Salpeter IMF.

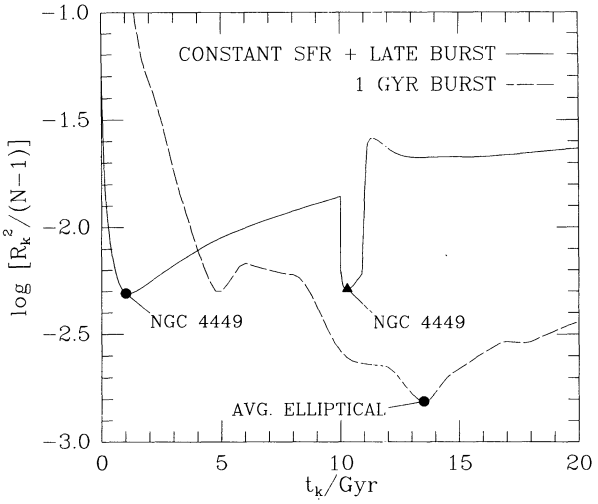

FIG. 8.—Sum of squared residuals between model and observed spectra (eq. [3]) as a function of time. The dashed line shows the comparison between the 1 Gyr burst model and the average spectrum of an elliptical galaxy. The minimum at 13.5 Gyr (*filled circle*) corresponds to the fit in Fig. 5. The solid line shows the comparison between a model of constant star formation rate, which doubles after 10 Gyr for a duration of 1 Gyr, and the spectrum of NGC 4449. The minimum at 1 Gyr (*filled circle*) corresponds to the fit in Fig. 6. The minimum after 10 Gyr (*triangle*) gives a similarly good fit to the observed spectrum.

tion with time of the sum of squared residuals (eq. [3]) between the models and the spectra of the average elliptical galaxy and of NGC 4449. Even though the 1 Gyr burst model reproduces best the average spectrum of an elliptical galaxy at 13.5 Gyr (Fig. 5), ages in the range 11–15 Gyr produce almost equally good fits, as stars with decreasing mass evolving off the main sequence conspire to maintain a roughly constant spectrum (see Fig. 4*a*). We note that the inclusion of convective overshooting on the stellar tracks is important mainly for turnoff ages younger than about 10 Gyr (§ 2.1) and thus has no effect on these numbers. To evaluate the significance of the age assigned to the spectrum of NGC 4449, we have considered a model with constant star formation rate which at age 10 Gyr increases by a factor of 2 for a duration of 1 Gyr. Because this late burst dominates the spectrum even though it only increases the stellar mass of the model by 10%, the fit of NGC 4449 around 10 Gyr is virtually identical to that obtained in Figure 6 around 1 Gyr. Similarly, one can show that the ages and star formation time scales of typical Sb–Sc galaxies are not rigidly constrained by the observed spectra in Figure 7, as fits like those presented could be obtained with shorter or longer star formation time scales at younger or older model ages, respectively.

Hence, the isochrone synthesis models can reproduce reasonably well the observed spectra or photometric properties from the UV to the near-IR of nearby galaxies of various Hubble types, in which young massive stars, old low-mass stars, or mixtures of stars of all masses and ages produce the light. These models therefore constitute a reliable means of investigating the spectral evolution of any stellar population dominated by solar metallicity stars. However, the spectral energy distributions alone do not permit the unambiguous determination of the age of a stellar population.

3.5. *Contribution of Different Stellar Groups*

We analyze here the contribution of stars in various evolutionary stages to the integrated spectrum of a stellar population. We consider the case of a 1 Gyr burst population at age 13.5 Gyr and compare it with a stellar population of constant star formation rate at the same age.

In Figure 9 we indicate the contributions to the total spectral energy distribution of the 1 Gyr burst model, at 13.5 Gyr, of stars in eight groups (the turnoff mass at 13 Gyr is about 0.85 $M_\odot$): main sequence (MS), subgiant branch (SGB), red giant branch (RGB), core He burning (CHeB), planetary nebula (PN), bare PN nucleus (PNN), and white dwarf (WD).

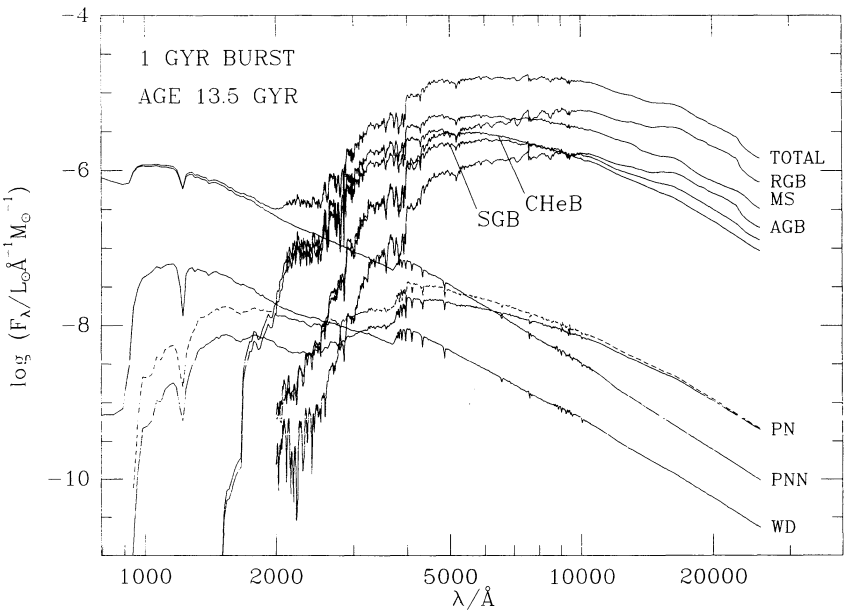

FIG. 9.—Contribution of stars in different groups to the total spectral energy distribution of a 1 Gyr burst population with the Salpeter IMF at age 13.5 Gyr. The acronyms are defined in § 3.5. The dashed line next to the PN contribution corresponds to the case where extinction of the core radiation by the surrounding nebula is ignored. The vertical scale corresponds to a total mass in stars of 1 $M_\odot$.

The spectrum blueward of 2000 Å is entirely dominated by low-mass post-AGB stars whose envelopes have dispersed. Main-sequence and subgiant stars account for most of the light between 3000 and 4000 Å, and the red giants produce more than half of the light at longer wavelengths. The exact shape of the spectrum from the optical to the near-IR, however, is a subtle combination of various nearly equivalent contributions. Note that planetary nebulae have a negligible contribution to the integrated spectrum, even if one ignores the absorption by the envelope of the core radiation (*dashed line*).

When star formation remains constant, the spectral energy distribution after 13.5 Gyr contrasts with the previous one by the much smaller importance of evolved stars with low-mass progenitors (Fig. 10). Massive stars on the main sequence strongly dominate the spectrum blueward of 5000 Å. From 5000 Å to about 1 μm, the main-sequence contribution drops from 60% to 30%, the red supergiants (CHeB) produce 30% of the light, while the AGB and red giant branch each account for half of the remaining light. Longward of 1 μm, the supergiant, AGB, and giant stars contribute roughly in equal amounts to the spectrum, while the main-sequence contribution continues to drop. Since the AGB contribution is mainly accounted for by intermediate-mass stars that have evolved in the last Gyr or so, the old stellar component is thus only apparent through the 30% contribution of the red giant branch to the near-infrared light. Reducing the proportion of massive stars in the IMF would naturally increase the importance of old stars in the spectrum.

The spectra shown in Figures 9 and 10 result predominantly from the addition of stellar spectra taken from the UV and IR extended version of the Gunn & Stryker atlas built as described in § 2.1. The contribution of the Kurucz (1979) models or the blackbody distributions used for the hottest stars is significant only shortward of 2000 Å.

4. INDICATORS OF SPECTRAL EVOLUTION

In this section we are interested in the indicators of spectral evolution that can be drawn from the isochrone synthesis models. In particular, we analyze the predicted evolution as a function of redshift of several broad-band colors and spectral discontinuities for a representative range of model galaxies, and compare them with a few observations. Our aim here is to give an overview of the range of possibilities offered by the new models rather than to make specific cosmological predictions using particular sets of data and models. These outgrowths of our work would overstep the scope of the present paper and are being developed elsewhere.

4.1. *Redshift-Color Relation*

In Figure 11 we present the $B-V$ and $V-K$ color evolution as a function of redshift of a representative range of isochrone synthesis models (these curves include both evolution and k-correction). We have considered two assumptions on the star formation rate, 1 Gyr burst (*solid lines*) and constant (*dashed lines*); two assumptions on the redshift of formation, $z_f = 1$ and $z_f = 30$; and two assumptions on the cosmological deceleration parameter, $q_0 = 0.5$ (*thick lines*) and $q_0 = 0$ (*thin lines*), for $H_0 = 50$ km s^{-1} Mpc^{-1}. The above range of star formation rates represents well the spread in star formation histories of nearby galaxies of various morphological types as inferred from their spectrophotometric properties (CB91 and § 3.4). Also shown in Figure 11 are the k-corrected colors of the average elliptical (*squares*) and the young irregular (*triangles*) galaxies studied in § 3.4 (no evolution included), which at $z = 0$ illustrate the color range spanned by nearby galaxies.

As expected, the 1 Gyr burst models forming at $z_f = 30$ fit the colors of the k-corrected elliptical galaxy after about 13 Gyr of evolution (i.e., at $z \approx 0$ for $q_0 = 0.5$, and at $z \approx 0.4$ for $q_0 = 0$), and the colors of the observed irregular can be fitted after 1 Gyr of constant star formation (at $z \approx 0.8$ for $z_f = 1$). From about 13 to 19 Gyr, the 1 Gyr burst model with $z_f = 30$ and $q_0 = 0$ roughly behaves like a nonevolving elliptical, but models forming at $z_f = 1$ are only 8 to 10 Gyr old at $z = 0$, depending on the cosmology, and are therefore slightly bluer. This result is independent of the duration of the initial burst, because the optical/near-IR colors are independent of the

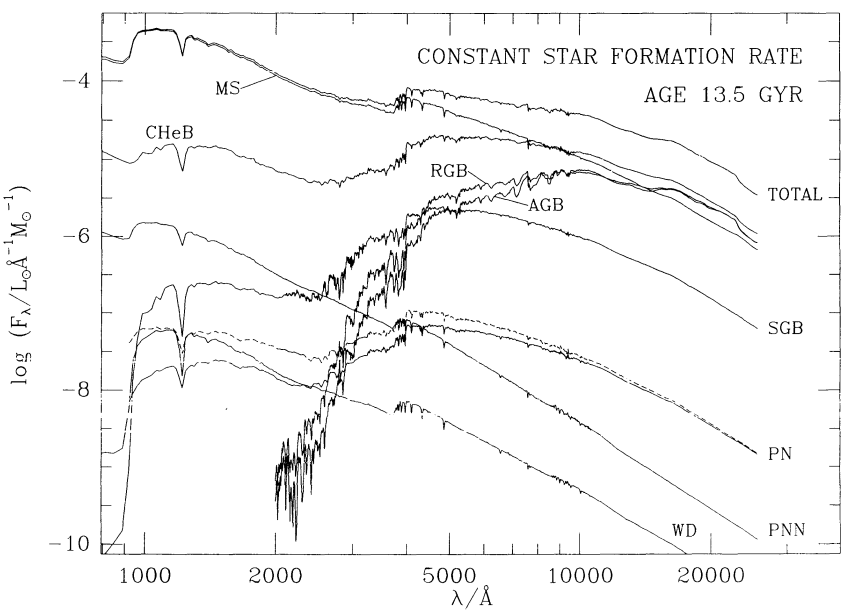

FIG. 10.—Same as Fig. 9 for a stellar population with constant star formation rate at age 13.5 Gyr

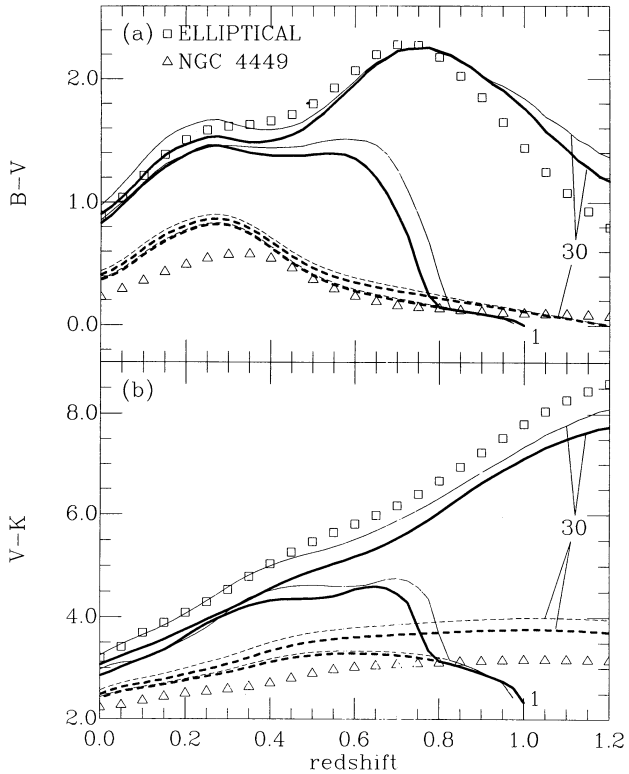

FIG. 11.—(*a*) Evolution of the $B-V$ color as a function of redshift as predicted by the isochrone synthesis model for two assumptions on the star formation rate, 1 Gyr burst (*solid lines*) and constant (*dashed lines*); two assumptions on the cosmological deceleration parameter, $q_0 = 0.5$ (*thick lines*) and $q_0 = 0$ (*thin lines*); and two assumptions on the redshift of formation, $z_f = 1$ and $z_f = 30$ (indicated on the figure), for $H_0 = 50$ km s^{-1} Mpc^{-1}. (*b*) Same as (*a*), but for the $V-K$ color. In both panels the squares and the triangles indicate the *k*-corrected colors of, respectively, the average elliptical galaxy and the blue irregular galaxy of Figs. 5 and 6.

details of the star formation episode once it has ceased for several billion years (see Fig. 6 of CB91). Note that the 1 Gyr burst models forming at $z_f = 30$ are redder than the non-evolving elliptical at redshifts $z \gtrsim 1$, because the B band samples the rest-frame $\lesssim$2500 Å light, and the UV-rising branch (present in the *k*-corrected elliptical) has not yet fully grown. Models with constant star formation rate, on the other hand, show very similar color-redshift relations over a wide range of redshifts of formation and cosmologies. This results from the prominence of massive stars in the spectrum at all ages (see § 3.4).

In Figure 12 we compare the $B-V$ and $V-R$ color-redshift relations of two of the isochrone synthesis models in Figure 11 (1 Gyr burst and constant star formation rate, for $z_f = 30$, $q_0 = 0.5$, and $H_0 = 50$ km s^{-1} Mpc^{-1}) with earlier predictions (Bruzual 1983; Guiderdoni & Rocca-Volmerange 1987; Bruzual 1987; see discussion in § 2.3).[7] For reference, the adopted cosmology implies that all models are 4 Gyr old at $z \approx 1.2$, 5 Gyr old at $z \approx 0.8$, 10 Gyr old at $z \approx 0.2$, and 13 Gyr old at $z \approx 0$. For practical reasons we have adopted in all models the three-segment IMF used by Guiderdoni & Rocca-Volmerange, which has an upper cutoff $m_U = 80\ M_\odot$. The resulting $B-V$ color of the 1 Gyr burst model (isochrone synthesis) is almost identical to that with $m_U = 125\ M_\odot$ in Figure 11 (because all massive stars have died at higher redshift), but, as expected, the lower IMF cutoff implies a redder $B-V$ in the case of constant star formation.

The various models in Figure 12 rely on different stellar spectra and different stellar evolutionary tracks. The influence of the stellar spectra alone can be isolated by comparing the Bruzual 1983 (*dashed lines*) and 1987 (*thin solid lines*) models, in which the evolutionary tracks are identical (see § 2.3). The $B-V$ and $V-R$ colors are very similar in both models, the largest discrepancy reaching $\sim$0.1 mag around $z \approx 0.3$. The colors are far more sensitive to the choice of the stellar evolutionary tracks. For instance, the differences between the Bruzual (1983, 1987) models and the isochrone synthesis model (*thick solid lines*) result from a combination of several effects which act in different directions: first, the lack of AGB and core He-burning stars in the Bruzual models leads to bluer colors than in the isochrone synthesis model, especially prior to the rise of the red giant branch (see $V-R$ color of the 1 Gyr burst model at $z \gtrsim 0.8$). But the Bruzual models do not include post-AGB stars either. This results in a redder $B-V$ color than predicted by the isochrone synthesis model when the B band falls blueward of $\lesssim$2500 Å in the rest frame (see 1 Gyr burst

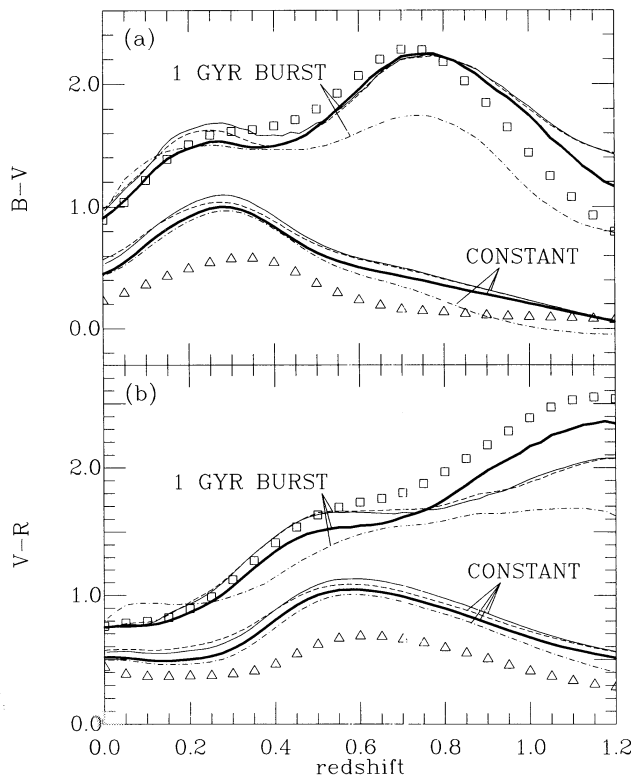

FIG. 12.—(*a*) Evolution of the $B-V$ color as a function of redshift as predicted by Bruzual (1983; *dashed lines*), Bruzual (1987; *thin solid lines*), Guiderdoni & Rocca-Volmerange (1987; *dot-dash lines*), and the present models of isochrone synthesis (*thick solid lines*), for two assumptions on the star formation rate, 1 Gyr burst and constant (indicated on the figure), and for $q_0 = 0.5$, $z_f = 30$, and $H_0 = 50$ km s^{-1} Mpc^{-1}. (*b*) Same as (*a*), but for the $V-R$ color. The squares and triangles have the same meanings as in Fig. 11. All models have the IMF slope and upper cutoff of 80 $M_\odot$ used by Guiderdoni & Rocca-Volmerange.

[7] The $V-R$ color was preferred over the $V-K$ color in this comparison, because the spectrum redward of 1 μm is interpolated between broad-band fluxes in the models of Bruzual (1983) and Guiderdoni & Rocca-Volmerange (1987).

model at $z \gtrsim 1$). The lengthening of main-sequence lifetimes by convective overshooting in the isochrone synthesis models also tends to blue the colors with respect to the Bruzual models. This effect, however, is much stronger for high-mass stars; thus for constant star formation the isochrone synthesis model is bluer than the Bruzual models at all ages. Furthermore, all stars less massive than 1.7 $M_\odot$ in the Bruzual models are assigned a common post–main-sequence evolution on the red giant branch of Tinsley & Gunn (1976). In the isochrone synthesis models, the red giant branch evolves toward cooler temperature and the duration of the post–main-sequence evolution increases with decreasing turnoff mass. As a result, the isochrone synthesis (1 Gyr burst) model reddens faster than the Bruzual models at late ages. This reddening is also accentuated by the absence of convective overshooting in stars less massive than about 1 $M_\odot$ (turnoff age $\gtrsim 10$ Gyr).

The differences between the model of Guiderdoni & Rocca-Volmerange (1987; *dot-dash lines*) and the isochrone synthesis model are also caused by the different stellar tracks used, since both models rely on similar spectra in the visible. The colors are much bluer in Guiderdoni & Rocca-Volmerange than in the isochrone synthesis model at high redshift, indicating a significant excess of rest-frame ultraviolet light. This excess must be attributed to a different prescription for the evolution of main-sequence stars, since Guiderdoni and Rocca-Volmerange did not include hot PNNs in their model. However, the exact cause cannot be traced clearly because these authors interpolated solar metallicity tracks from tracks with nonsolar metallicity (Mengel et al. 1979; Sweigart & Gross 1978), without giving details, for stars with masses lower than 2.2 $M_\odot$ (main-sequence lifetimes $\gtrsim 1$ Gyr). At lower redshifts the models of Guiderdoni & Rocca-Volmerange are too red, because they rely on the prescription of Renzini & Voli (1981), who overestimated the contribution of AGB stars after 2×10^9 yr (see Fig. 4 of CB91). Since these stars become less prominent at very late ages, the 1 Gyr burst model of Guiderdoni & Rocca-Volmerange also fits the colors of the average elliptical galaxy around $z \approx 0$.

Interestingly, then, even though all the 1 Gyr burst models in Figure 12 roughly match the $B-V$ and $V-R$ colors of an observed elliptical galaxy at $z \approx 0$, the predicted color-redshift relations differ widely from one model to another. The isochrone synthesis model has so far the advantage of reproducing well the optical/near-IR colors of stellar populations in a wide range of ages and star formation histories.

4.2. *Spectral Discontinuities*

Discontinuities in the integrated spectra of stellar populations, such as the Lyman break at 912 Å or the 4000 Å break, are characteristic of the most prominent stars and can thus be used as tracers of evolution (Bruzual 1983; Hamilton 1985; Spinrad 1986). We show in Figure 13 the predicted evolution of these two discontinuities in stellar populations with various time scales of star formation according to the isochrone synthesis models. We have adopted the definitions (Bruzual 1983)

$$B_\nu(912\ \text{Å}) = \int_{1000}^{1100} d\lambda\, F_\nu(\lambda) \Big/ \int_{800}^{900} d\lambda\, F_\nu(\lambda) \qquad (4)$$

and

$$B_\nu(4000\ \text{Å}) = \int_{4050}^{4250} d\lambda\, F_\nu(\lambda) \Big/ \int_{3750}^{3950} d\lambda\, F_\nu(\lambda)\,, \qquad (5)$$

where the ranges of integration are in angstroms.

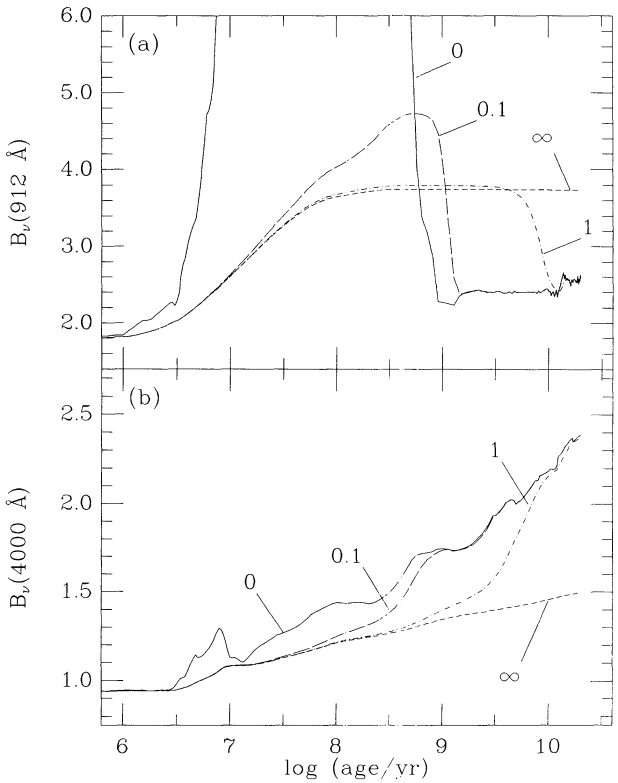

FIG. 13.—(*a*) Amplitude of the 912 Å spectral discontinuity (eq. [4]) as a function of the age in four isochrone synthesis models with different time scales of star formation (indicated in Gyr next to the curves): instantaneous burst (*solid line*); constant (*short-dashed line*); eq. (2) with $\tau = 0.1$ Gyr (*long-dashed line*); eq. (2) with $\tau = 1$ Gyr (*dot-dash line*). The amplitude reaches about 1000 around 1×10^8 yr in the instantaneous-burst model (see text). (*b*) Same as (*a*), but for the 4000 Å spectral discontinuity (eq. [5]).

The amplitude of the 912 Å break in the instantaneous-burst stellar population (Fig. 13*a*, *solid line*) rises rapidly as the most massive stars evolve off the main sequence (reaching about 1000 around 1×10^8 yr). After the turnoff mass drops below 7 $M_\odot$ (around 4×10^7 yr), hot PNNs start supplying new ionizing radiation, but the break amplitude decreases substantially only after about 1×10^9 yr (turnoff mass 2.5 $M_\odot$) when evolved stars spend more time on the post-AGB. When star formation takes place over longer time scales, the dispersion in stellar age washes out the rapid evolution of the 912 Å break at early epochs. However, a deep 912 Å break in real galaxies does not necessarily imply short time scales of star formation, since it could also be due to absorption by neutral hydrogen of stellar ionizing photons. Unlike the 912 Å break, the 4000 Å break in the instantaneous-burst population is controlled by the most massive stars on the main sequence, and increases monotonically as the turnoff mass decreases, from about 1×10^7 yr to about 10 Gyr (Fig. 13*b*). During the supergiant phase prior to 1×10^7 yr, massive stars evolve at very high luminosities and make the break rise substantially. After 10 Gyr, the contribution of red giants becomes important around 4000 Å and accentuates the increase of the break. Both the 912 Å break and the 4000 Å break are insensitive to the exact duration of the star formation episode once it has ceased for several billion years.

We compare in Figure 14 the predicted amplitude of the 4000 Å break of a 1 Gyr burst population with the amplitudes measured in a sample of red galaxies at redshifts $0 \lesssim z \lesssim 0.8$ (Hamilton 1985; Spinrad 1986). We have made the same

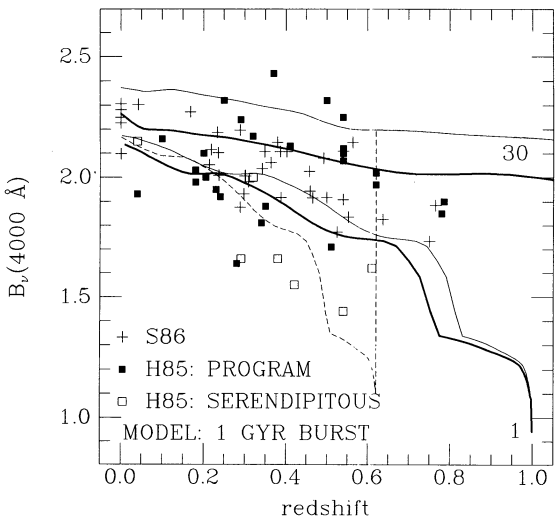

FIG. 14.—Amplitude of the 4000 Å spectral discontinuity of a 1 Gyr burst model as a function of redshift for two assumptions on the redshift of formation, $z_f = 1$ and $z_f = 30$ (indicated on the figure), and two assumptions on the cosmological deceleration parameter, $q_0 = 0.5$ (*thick solid lines*) and $q_0 = 0$ (*thin solid lines*), for $H_0 = 50$ km s^{-1} Mpc^{-1}. Also shown are the observations of Hamilton (1985), for which a distinction has been made between program galaxies (*filled squares*) and serendipitous galaxies (*open squares*), and the observations of Spinrad (1986; *plus signs*). The dashed line corresponds to a model forming 50% of its stars in a 1 Gyr burst at $z_f = 30$ and 50% in a 0.5 Gyr burst at $z = 0.6$, for $q_0 = 0$.

assumptions as earlier on the redshift of formation and the cosmology (*thin and heavy solid lines*). Many of the galaxies (including all serendipitous objects observed by Hamilton around $z \sim 0.5$) have too shallow breaks to be fitted by even the young model corresponding to $z_f = 1$ and $q_0 = 0.5$. This may indicate either a more recent episode of star formation or a metallicity lower than solar. In fact, these data can be reproduced by a model that forms 50% of its stars in a 1 Gyr burst at $z_f = 30$ and 50% in a 0.5 Gyr burst at $z = 0.6$, for $q_0 = 0$ (*dashed line*). Note also that some observed breaks in Figure 14 are too deep to be fitted by the oldest models. These data could correspond to stellar populations with metallicities higher than solar.

5. SUMMARY AND CONCLUSION

We have supplemented the isochrone synthesis model of CB91 with an updated library of spectra for solar metallicity stars, to predict the spectral evolution of stellar populations. In doing so, we have introduced three significant improvements over earlier work. First, the library of stellar spectra assembled here includes observed near-IR spectra from 1.22 to 2.56 μm of stars in a wide range of spectral types and luminosity classes. Other published models of spectral evolution approximated the spectra in the near-IR by coarse interpolation from broad-band fluxes (Bruzual 1983; Guiderdoni & Rocca-Volmerange 1987). Second, our assignment of observed spectra to locations on the evolutionary tracks in the CMD is based on optical/near-IR color calibrations. This ensures a better representation of the light at all wavelengths than in models where the spectra are selected from the $B-V$ color or the effective temperature of the stars alone (Bruzual 1983, 1987; Guiderdoni & Rocca-Volmerange 1987). As a result, we find excellent agreement between the optical/near-IR properties of the new spectroscopic models and the predictions of purely photometric models computed with the same library of stellar tracks. Third, we have supplemented the spectral library with model atmospheres of very hot stars for which observed spectra were not available. We also used appropriate color calibrations for stars with circumstellar shells and dusty envelopes.

We have revised the main-sequence lifetimes of stars with masses in the range $1.3\ M_\odot \leq m \leq 2.5\ M_\odot$ as recently prescribed by Maeder & Meynet (1991). While this does not affect at all our discussion in CB91 of the advantages and disadvantages of various approaches to population synthesis, we conclude that the new tracks confirm and even improve the agreement presented in CB91 of the photometric models of isochrone synthesis with the optical/near-IR properties of nearby stellar populations in a wide range of ages and star formation histories. Furthermore, we conclude from our present analysis of the spectral evolution that models with various time scales of star formation reproduce well the observed spectra of nearby elliptical and spiral galaxies after several billion years of evolution. In fact, only "spectral synthesis" can so far reproduce as accurately the observed spectra of early-type galaxies (e.g., Pickles & van der Kruit 1987).[8] Since the present isochrone synthesis models also reproduce well the typical spectral energy distribution of young irregulars (and the optical/near-IR colors of star clusters with ages in the range 0.01–4 Gyr), they constitute a reliable tool to study the spectrophotometric evolution of arbitrary stellar populations dominated by solar metallicity stars. As expected, the predicted evolution of the optical/near-IR colors as a function of redshift differ significantly from earlier predictions. Their consequences for our understanding of galaxy formation and evolution are being investigated.

We have also refined the library of stellar evolutionary tracks assembled in CB91 to describe more accurately the late evolution of low- and intermediate-mass stars as hot nuclei of planetary nebulae and through the white dwarf cooling sequence (Magris & Bruzual 1992). While stars in these stages contribute negligibly to the optical/near-IR light, we confirm with a self-consistent model that they can account for the UV flux observed in quiescent elliptical galaxies such as NGC 4472 (Burstein et al. 1988). Models that do not include post-AGB stars require additional star formation. The spectrum of quiescent elliptical galaxies like NGC 4649 also require continuing star formation within the framework of our solar metallicity isochrone synthesis models (Magris & Bruzual 1992).

The method of isochrone synthesis (CB91), because it involves an accurate interpolation of all evolutionary stages in the CMD, allows us to take full advantage of the improvements introduced by the updated libraries of stellar tracks and stellar spectra. The resulting success of the models at reproducing the UV/near-IR properties of nearby stellar populations constitutes a strong basis for future work. Priority will be given to including the effect of chemical evolution, as stellar evolutionary tracks and model atmospheres for nonsolar metallicity are becoming available. Finally, isochrone synthesis has the advantage of producing smoothly evolving properties of instantaneous-burst stellar populations, from which the properties of populations with arbitrary star formation rates

[8] The spectral synthesis approach of Pickles & van der Kruit (1987) consisted in computing synthetic spectra for a few isochrones at selected turnoff ages, and looking for the optimum combination of isochrones that would reproduce the spectra of early-type galaxies. This may be considered as a pioneer, more ad hoc version of the isochrone synthesis approach.

can be inferred. The predicted spectral evolution of several instantaneous-burst populations with different IMFs will be made available for general use in the near future.

We thank G. Magris for her active involvement in assembling the evolutionary tracks of post-AGB stars. S. E. Persson provided valuable unpublished data, program codes, and critical and interesting discussions. We also thank D. W. Strecker and collaborators for providing unpublished KAO Stellar spectra, and J. B. Oke for kindly sending us his spectrum of an average elliptical galaxy. We also thank the referee, S. M. Faber, for helpful and stimulating suggestions. CIDA and STScI are gratefully acknowledged for ample financial and computer support. S. C. also thanks the French Ministère de la Recherche et de la Technologie for partial support.

REFERENCES

Aaronson, M. 1978, ApJ, 221, L103
Bell, R. A., & Gustafsson, B. 1978, A&AS, 34, 229
Bertelli, G., Bressan, A., & Chiosi, C. 1992, ApJ, 392, 522
Bertelli, G., Chiosi, C., & Bertola, F. 1989, ApJ, 339, 889
Bessel, M. S., & Brett, J. M. 1988, PASP, 100, 1134
Böhm-Vitense, E. 1972, A&A, 17, 335
Bruzual A., G. 1983, ApJ, 273, 105
———. 1987, unpublished
———. 1991, in IAU Symp. 149, The Stellar Populations of Galaxies, ed. B. Barbuy & A. Renzini (Dordrecht: Kluwer), 311
Buonanno, R. 1986, Mem. Soc. Astron. Italiana, 57, 333
Burstein, D., Bertola, F., Buson, L. M., Faber, S. M., & Lauer, T. R. 1988, ApJ, 328, 440
Buser, R. 1978, A&A, 62, 411
Buser, R., & Kurucz, R. L. 1978, A&A, 70, 555
Buzzoni, A. 1990, ApJS, 71, 817
Charlot, S., & Bruzual A., G. 1991, ApJ, 367, 126 (CB91)
Chiosi, C. 1990, private communication
Code, A. D., Davis, J., Bless, R. C., & Hanbury Brown, R. 1976, ApJ, 203, 417
Code, A. D., Holm, A. V., & Bottemiller, R. L. 1980, ApJS, 43, 501
Code, A. D., & Meade, M. R. 1979, ApJS, 39, 195
Davies, R. L., Burstein, D., Dressler, A., Faber, S. M., Lynden-Bell, D., Terlevich, R. J., & Wegner, G. 1987, ApJS, 64, 581
Eggen, O. J., & Sandage, A. R. 1964, ApJ, 140, 130
Ellis, R. S. E., & Bruzual A., G. 1983, unpublished
Elson, R. A. W., & Fall, S. M. 1988, AJ, 96, 1383
Faber, S. M., Friel, E. D., Burstein, D., & Gaskell, C. M. 1985, ApJS, 57, 711
Flower, P. J. 1977, A&A, 54, 31
Gilliland, R. L., et al. 1991, AJ, 101, 541
Greggio, L., & Renzini, A. 1990, ApJ, 364, 35
Guiderdoni, B., & Rocca-Volmerange, B. 1987, A&A, 186, 1
Gunn, J. E., & Stryker, L. L. 1983, ApJS, 52, 121
Gunn, J. E., Stryker, L. L., & Tinsley, B. M. 1981, ApJ, 249, 48
Hamilton, D. 1985, ApJ, 297, 371
Heck, A., Egret, D., Jaschek, M., & Jaschek, C. 1984, *IUE* Low-Dispersion Spectral Reference Atlas (ESA SP-1052; Paris: ESA), 1
Iben, I., Jr., & Truran, J. W. 1978, ApJ, 220, 980
IRAS Point Source Catalog. 1985, Joint *IRAS* Science Working Group (Washington, DC: GPO)
Janes, K. A. 1985, in IAU Symp. 111, Calibration of Fundamental Stellar Quantities, ed. D. S. Hayes, L. E. Pasinetti, & A. G. D. Philip (Dordrecht: Reidel), 361
Janes, K. A., & Smith, G. H. 1984, AJ, 89, 487
Johnson, H. L. 1965, ApJ, 141, 923
———. 1966, ARA&A, 4, 193
Kennicutt, R. C. 1992, ApJS, 79, 255
Kurucz, R. L. 1979, ApJS, 40, 1
Lawson, C. L., & Hanson, R. J. 1974, in Solving Least Squares Problems (Englewood Cliffs: Prentice-Hall), 158
Maeder, A., & Meynet, G. 1989, A&A, 210, 155
———. 1991, private communication
Magris C. G., & Bruzual A., G. 1991, in IAU Symp. 149, The Stellar Populations of Galaxies, ed. B. Barbuy & A. Renzini (Dordrecht: Kluwer), 452
Magris C. G., & Bruzual A., G. 1992, in preparation
Meade, M. R., & Code, A. D. 1980, ApJS, 42, 283
Mengel, J. G., Sweigart, A. V., Demarque, P., & Gross, P. G. 1979, ApJS, 40, 733
Micela, G., Sciortino, S., Vaiana, G. S., Schmitt, J. H. M. M., Stern, R. A., Harnden, F. R., Jr., & Rosner, R. 1988, ApJ, 325, 798
O'Connell, R. W. 1986, in Stellar Populations, ed. C. A. Norman, A. Renzini, & M. Tosi (Cambridge: Cambridge Univ. Press), 167
Pandey, A. K., Bhatt, B. C., Mahra, H. S., & Sagar, R. 1989, MNRAS, 236, 263
Persson, S. E. 1987, unpublished
Persson, S. E., Aaronson, M., Cohen, J. G., Frogel, J. A., & Matthews, K. 1983, ApJ, 266, 105
Persson, S. E., Oke, J. B., Porter, A. C., Matthews, K., Gunn, J. E., & Bruzual A., G. 1992, in preparation
Peterson, D. M., & Solensky, R. 1988, ApJ, 333, 256
Pickles, A. J., & van der Kruit, P. C. 1987, in Towards Understanding Galaxies at Large Redshifts, ed. R. G. Kron & A. Renzini (Dordrecht: Reidel), 29
Pottasch, S. R. 1984, in Planetary Nebulae (Dordrecht: Reidel), 199
Racine, R. 1971, ApJ, 168, 393
———. 1973, AJ, 78, 180
Renzini, A. 1981, Ann. Physique, 6, 87
Renzini, A., & Buzzoni, A. 1986, in Spectral Evolution of Galaxies, ed. C. Chiosi & A. Renzini (Dordrecht: Reidel), 195
Renzini, A., & Voli, M. 1981, A&A, 94, 175
Ridgway, S. T., Joyce, R. R., White, N. M., & Wing, R. F. 1980, ApJ, 235, 126
Salpeter, E. E. 1955, ApJ, 121, 161
Sandage, A. 1982, ApJ, 252, 553
Savage, B. D., & Mathis, J. S. 1979, ARA&A, 17, 73
Schaller, G., Schaerer, D., Meynet, G., & Maeder, A. 1992, A&AS, in press
Schönberner, D. 1981, A&A, 103, 119
———. 1983, ApJ, 272, 708
———. 1986, A&A, 169, 189
Spergel, D. N., Giuliani, J. L., Jr., & Knapp, G. R. 1983, ApJ, 275, 330
Spinrad, H. 1986, PASP, 98, 269
Straižys, V., & Sviderskiene, Z. 1972, Bull. Vilnius Astron. Obs., 35, 1
Strecker, D. W., Erickson, E. F., & Witteborn, F. C. 1979, ApJS, 41, 501
———. 1989, unpublished
Sweigart, A. V., & Gross, P. G. 1978, ApJS, 36, 405
Taylor, B. J., & Joner, M. D. 1990, AJ, 100, 830
Tinsley, B. M. 1980, ApJ, 241, 41
Tinsley, B. M., & Gunn, J. E. 1976, ApJ, 203, 52
Upgren, A. R. 1974, ApJ, 193, 359
Upgren, A. R., & Weis, E. W. 1977, AJ, 82, 978
van den Bergh, S. 1981, A&A, 46, 79
Weidemann, V. 1987, A&A, 188, 74
———. 1990, ARA&A, 28, 103
Worthey, G., Faber, S. M., & Gonzalez, J. J. 1992, ApJ, 398, 69
Wu, C. C., et al. 1983, NASA IUE Newsletter, 22, 1
Wu, C. C., Crenshaw, D. M., Blackwell, Jr., J. H., Wilson-Diaz, D., Schiffer, F. H., III, Burstein, D., Fanelli, M. N., & O'Connell, R. W. 1991, NASA IUE Newsletter, 43, 1
Yee, H. K. C., & Oke, J. B. 1978, ApJ, 226, 753
Zinn, R. 1986, in Stellar Populations, ed. C. A. Norman, A. Renzini, & M. Tosi (Cambridge: Cambridge Univ. Press), 73